Polyaromatic Compounds Hot Paper

Deutsche Ausgabe: DOI: 10.1002/ange.201608400
Internationale Ausgabe: DOI: 10.1002/anie.201608400

An Electron-Deficient Azacoronene Obtained by Radial π Extension

*Marika Żyła-Karwowska, Halina Zhylitskaya, Joanna Cybińska, Tadeusz Lis, Piotr J. Chmielewski, and Marcin Stępień**

Abstract: *A hexapyrrolohexaazacoronene derivative containing 37 fused rings, the largest such system to date, was obtained from a naphthalenomonoimide–pyrrole hybrid in a concise and efficient synthesis. This large heterocycle is electron-deficient and shows extended redox activity, spanning at least 13 oxidation levels, but is otherwise chemically stable. Radial expansion of the π system creates a chromophore characterized by strong fluorescence and solvatochromism in the neutral state, and strong near-infrared absorption in the charged states. Additionally, the enlarged and ruffled aromatic surface supports a unique self-assembly mode in the crystal, leading to the formation of highly solvated organic clathrates.*

The development of nanoscale molecular analogs of graphene is one of the topical areas of current aromatic chemistry. Such objects can be constructed as formal subsections of the graphene sheet (nanographenes), but they can be also fashioned to contain heteroatoms or non-benzenoid rings.[1,2] Both of these features are present in members of the azacoronene family, an emerging class of nanographene analogs.[3–6] The parent system, hexapyrrolohexaazacoronene (HPHAC, Scheme 1), first characterized by Müllen and coworkers,[3] can be seen as a pyrrole-based analog of hexa-*peri*-hexabenzocoronene (HBC). Further examples of azacoronene analogs were subsequently reported, containing complex patterns of five-, six-, and seven-membered rings.[4–6] These azacoronenes are very electron-rich, with up to six accessible oxidation levels.

Working in a complementary area of aromatic chemistry, we have recently proposed a new paradigm for creating tunable, electron-deficient oligopyrrole structures,[7] which may be of interest as *n*-type channel organic semiconductors[8–10] redox-active NIR chromophores,[11] or charge-storage materials.[12,13] In particular, we have shown that a system obtained by fusing four naphthalenemonoimide units (NMI, Scheme 1) to a porphyrin ring could be chemically and electrochemically reduced up to the octaanion level. Here we show that the synthetic use of this modular strategy is not limited to aldehyde–pyrrole condensations and that electron-deficient pyrrole building blocks can be successfully employed in the nucleophilic substitution–oxidative coupling sequence used in azacoronene chemistry. This approach provides ready access to a uniquely large, radially fused HPHAC derivative with an extended redox behavior covering at least 13 oxidation levels.

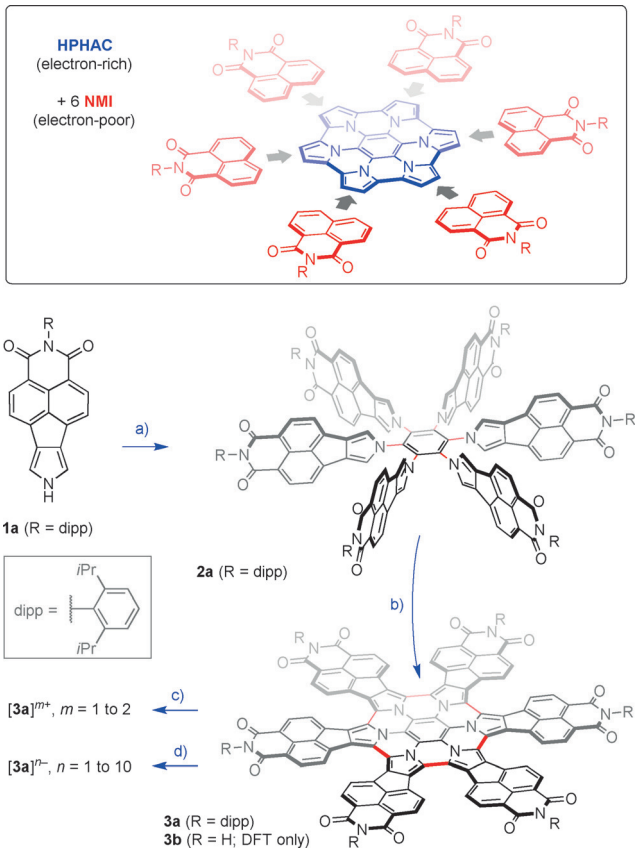

Scheme 1. Design and synthesis of the radially extended HPHAC analog **3a**. Reagents and conditions: a) 1. NaH, *N*,*N*-dimethylformamide (DMF), 20 °C; 2. C_6F_6, 50 °C, 12 h. b) $FeCl_3$ (36 equiv), CH_2Cl_2, 50 °C, 1 h. c) $(NO)[SbF_6]$, CH_2Cl_2. d) Sodium anthracenide, THF.

The NMI-fused pyrrole **1a**,[7] bearing a bulky 2,6-diisopropylphenyl (dipp) group on the imide nitrogen for improving solubility, was selected as the preferred building block, as it had been previously observed to combine an electron-poor character with good chemical stability. **1a** was condensed with hexafluorobenzene, in the presence of sodium hydride,[14] yielding the π-extended hexapyrrolylbenzene **2a** (Scheme 1). The latter precursor was subjected to oxidative coupling using $FeCl_3$, to produce the fully coupled, radially extended HPHAC **3a**. In spite of the electron-deficient character of the NMI–pyrrole subunits, the oxidation pro-

[*] M. Żyła-Karwowska, Dr. H. Zhylitskaya, Dr. J. Cybińska, Prof. T. Lis, Prof. P. J. Chmielewski, Prof. M. Stępień
Wydział Chemii, Uniwersytet Wrocławski
ul. F. Joliot-Curie 14, 50-383 Wrocław (Poland)
E-mail: marcin.stepien@chem.uni.wroc.pl
Homepage: http://www.mstepien.edu.pl
Dr. J. Cybińska
Wrocławskie Centrum Badań EIT+
ul. Stabłowicka 147, 54-066 Wrocław (Poland)

Supporting information for this article can be found under: http://dx.doi.org/10.1002/anie.201608400.

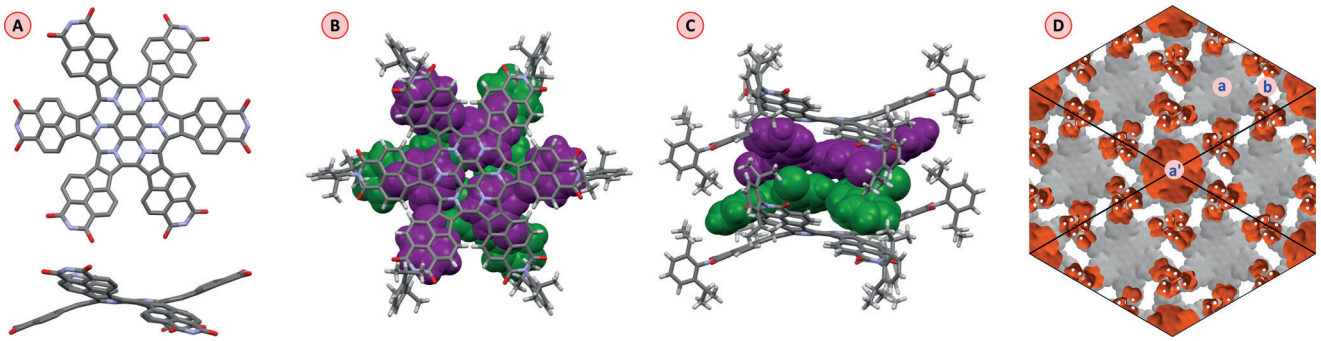

Figure 1. X-ray crystallographic analysis of **3a**·24 C_6H_5Cl. A) Perspective view with hydrogen atoms, dipp groups, and solvent molecules removed for clarity. B,C) Assembly of 12 chlorobenzene molecules sandwiched between two molecules of **3a**. Only the major disorder positions are shown for chlorobenzene. The green and purple layers are related by an inversion center. D) Crystal voids (procrystal density, 0.002 a.u. isosurface) as seen along the *c* direction. **3a** and solvent molecules are located, respectively, on the orange and gray sides of the isosurface.

ceeded smoothly, although gentle heating was needed to effect the complete fusion of the periphery. The identity of the product was initially confirmed by a mass spectrum, which revealed the molecular ion at $m/z = 2574.9658$, corresponding to the molecular formula $C_{174}H_{126}N_{12}O_{12}$.

X-ray quality crystals of **3a** were grown by slow evaporation of a chlorobenzene–dichloromethane solution. In the crystal ($R\bar{3}$ space group), the molecule of **3a** occupies a −3 special position. The fused pyrrole subunits take alternating tilted positions relative to the mean plane of the nanographenoid (Figure 1 A), forming angles of 21° between the central benzene plane and the mean plane of each NMI subunit. The diameter of the molecule, measured between *para*-H atoms of two opposite dipp groups is about 32 Å, and the N-to-N diameter of the aromatic core is 22 Å. In the crystal, the molecules are stacked along the *c* direction, with intermolecular distances corresponding to the unit translation of 10.97 Å. Because the vertical extent of one molecule is about 17 Å, the dipp-NMI arms of consecutive molecules are partly interdigitated.

The crystals of **3a** are very highly solvated, enclathrating 24 molecules of chlorobenzene (CB) per molecule of **3a**. Two layers of six CB molecules each are enclosed between two molecules of **3a** (Figure 1 B,C), forming a unique "double burger" arrangement, whereas the remaining solvent occupies channels extending along the *c* direction. When CB molecules are artificially removed from the crystal structure model, the resulting voids occupy about 44 % of the cell volume (0.0003 a.u. pro-molecule density, Figure 1 D),[15] whereas the corresponding channel network is permeable to spherical probes of up to 2.0 Å radius (see Figure S3 in the Supporting Information).[16] The solvation level in **3a** is thus even higher than observed in crystals of the corresponding NMI-fused porphyrins derived from **1a**[7] and in fact, the total weight of entrapped CB exceeds the weight content of **3a** in the unit cell. The efficient enclathration of solvent by **3a** can be attributed to the combined contributions of the highly distorted aromatic core and the presence of bulky dipp groups, which all contribute to the formation of large internal molecular free volumes.[17,18]

Unlike many large nanographenes, **3a** is well soluble in chlorinated and aromatic solvents, a feature permitting its detailed characterization in solution. The NMR spectrum of **3a** in $CDCl_3$ is very simple, reflecting the six-fold symmetry axis of the molecule. In the aromatic region, there are two doublets at 8.80 and 7.90 ppm, corresponding to the naphthalene fragment, and an AB_2 system of the dipp group (7.50 and 7.35 ppm). The latter spin system and the presence of just one set of isopropyl signals (at 2.85 and 1.20 ppm) are consistent with an effective D_6h symmetry, suggesting that the saddle-like distortion of **3a**, observed in the solid state, undergoes rapid inversion in solution. No line broadening is observed, suggesting that π aggregation is not significant in the chloroform solution.

The electronic absorption spectrum of **3a** shows an intense band in the visible region (500 to 700 nm, ε_{max} up to $9.7 \times 10^4\,M^{-1}cm^{-1}$ in toluene; Figure S4 and Table S1), with a clearly visible vibronic pattern characteristic of many rylene imide derivatives.[19] The band evidently results from the interaction between HPHAC and NMI fragments, as it is absent in **2a** ($\lambda_{onset} < 500$ nm). **3a** exhibits considerable solvatochromism in solution, its color changing from purple in toluene, through bluish in dichloromethane, to bluish-gray in methanol. While the energy of the 0-0 transition shows relatively little solvent dependence (615, 620, 625 nm in toluene, dichloromethane (DCM), and MeOH, respectively), the relative intensities of higher vibronic components increase with solvent polarity, as does the overall broadening of the spectrum. The spectrum in MeOH features an absorption tail extending beyond 1100 nm, apparently associated with solvent-induced aggregation. In contrast to previously reported HPHAC derivatives, **3a** is strongly fluorescent (Figures S4–S10, Table S2). The emission is especially pronounced in nonpolar solvents ($\lambda_{max}^{em} = 659$ nm, $\Phi_F = 0.40$ in toluene) and becomes weaker and further red-shifted in more polar media, such as DCM ($\Phi_F = 0.27$) or MeOH ($\Phi_F < 0.03$). The vibronic structure is also broadened in polar solvents, paralleling the changes of absorption spectra. In frozen solutions at 77 K, the emission patterns become narrower and red-shifted relative to the room-temperature spectra. Emission lifetimes of **3a** were relatively short, up to ca 7.8 ns (toluene, 77 K).

Cyclic and differential pulse voltammetry experiments performed for **3a** revealed a complex multi-redox behavior (Figure 2 A). A single two-electron oxidation wave was

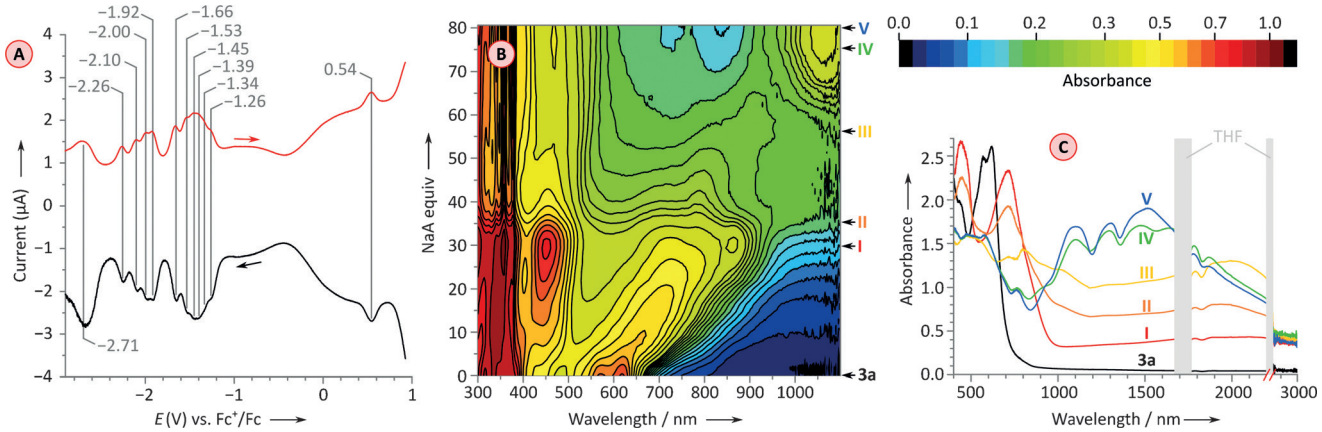

Figure 2. A) Differential pulse voltammetry of **3a** (THF, $NBu_4[BF_4]$). B) Titration of **3a** with sodium antracenide (NaA, THF). Contours and colors represent different absorbance values. NaA equivalents are given according to the initial anthracene concentration and are for reference only. C) Selected spectra observed during the reduction of **3a** with NaA, recorded in a separate titration experiment. The initial spectrum of **3a** is shown in black. Approximate positions of the corresponding titration stages (I to V) are indicated at the right edge of panel B.

identified in tetrahydrofuran (THF) solution at 0.54 V (vs. Fc^+/Fc^0), indicating that, in line with its electron-deficient character, **3a** is significantly more difficult to oxidize than aryl-substituted HPHACs, which have E_{ox}^1 in the range of −0.3 to 0.0 V.[3,5] In contrast to the latter systems, however, **3a** is an excellent electron acceptor, active over a broad range of potentials. Six overlapping reduction waves were identified between −1.26 V and −1.64 V, followed by four additional reductions at −2.00 V to −2.26 V, and a less clearly defined, possibly multi-electron event at ca. −2.7 V. The ability of a contiguously fused aromatic system to accept up to 10 electrons at moderately low potentials is a unique feature, surpassing the 8-electron reduction reported for the recently described zinc(II) porphyrin–NMI hybrid. The onset of reduction occurs in **3a** at a somewhat lower potential than in the latter porphyrin ($E_{red}^1 = -0.97$ V). The 10-electron reduction of **3a** corresponds to a charging capacity of 0.079 electrons per non-H atom, and is in fact slightly higher than in the NMI–porphyrin, which is only reduced to the hexaanion above −2.26 V (0.071 e per atom; 0.095 for the octaanion).[7]

3a was oxidized with nitrosonium hexafluoroantimonate in dichloromethane, yielding a diamagnetic dication $\mathbf{3a}^{2+}$, which showed enhanced diatropic characteristics in the ^{1}H NMR spectrum, indicated by the downfield NMI shifts at 9.51 and 9.02 ppm. Nucleus-independent chemical shift (NICS) calculations (Table S3) show that, in $\mathbf{3a}^{2+}$, the principal conjugation pathway contains 30 π electrons and encompasses the HPHAC substructure. The NMI units are thus deshielded by the inner ring current without directly participating in peripheral conjugation. A comproportionation experiment between **3a** and $\mathbf{3a}^{2+}$ (Figure S11) showed the formation of an intermediate species, not observed in voltammetry scans, which was identified as the radical cation $\mathbf{3a}^+$, on the basis of an ESR spectrum ($g = 2.0028$). The NIR signatures of $\mathbf{3a}^{2+}$ and $\mathbf{3a}^+$ consist of a relatively sharp absorption at 1050 and 1350 nm, respectively, followed by an extended band reaching up to 2200 nm ($\mathbf{3a}^{2+}$) and at least 2600 nm ($\mathbf{3a}^+$). These absorptions are qualitatively very similar to those reported for the corresponding cations of an aryl-substituted HPHAC,[3] but are shifted to wavelengths longer by several hundred nanometers. Overall, in the $\mathbf{3a}^{2+}$ and $\mathbf{3a}^+$ cations, the NMI units have a principally inductive effect on the electronic structure of the HPHAC core.

Under strictly oxygen- and moisture-free conditions, **3a** was chemically reduced with sodium anthracenide (NaA) in tetrahydrofuran (Figure 2B,C). A large and somewhat variable excess of NaA was needed for complete reduction of **3a**, and the endpoint of the titration was indicated by the rise of anthracenide absorptions. The titration showed multiple reduction events, which however were insufficiently well separated to permit identification of all species formed. The initial reduction phase (up to stage I, Figure 2C) was marked by an apparent shifting of the main absorption band of **3a** towards ca. 800 nm and a relatively slow increase of absorbance above 1000 nm. These changes correspond to at least five reaction events. Beyond that point, the NIR absorptivity increases considerably (stages II to V, ε_{max} up to ca. $6 \times 10^4\,M^{-1}\,cm^{-1}$). Interestingly, reduced solutions of **3a** show nonzero absorbance in a narrow spectral window between 2850 and 3000 nm available in THF, indicating that the optical band gaps of some of the anions may be smaller than 0.4 eV. Importantly, **3a** could be recovered from the anthracenide-reduced solutions by simple aerial oxidation. Clearly, the anions of **3a** are chemically more robust than those of the corresponding NMI–porphyrin, which were immediately decomposed by exposure to air.[7]

The reduction of **3a** with NaA was also monitored in $[D_8]$THF using ^{1}H NMR spectroscopy, but the only observable signals were those of anthracene and other NaA byproducts. The lack of well-resolved spectra of the expected **3a** anions was supposed to indicate that considerable amounts of paramagnetic species were present at all stages of the titration. Indeed, ESR spectroscopy showed the appearance of a strong radical signal immediately after addition of the first aliquot of NaA ($g = 2.0044$). During further titration, the signal intensity was reduced and a much weaker, broadened line was observed at $g = 2.0033$ (Figure S12). The asymmetry of the latter signal may be a result of high magnetic anisotropy

under slow tumbling conditions, or indicate the contribution of a triplet state. The signal intensity was decreasing with subsequent addition of the reductant, and upon reaching the endpoint, the expected multiplet of the anthracenide radical ion was observed. Thus, both NMR and ESR data are consistent with persisting paramagnetism of **3a** during anthracenide reduction.

The electronic characteristics of **3a**, discussed above, were convincingly rationalized using density functional theory (DFT). Kohn–Sham frontier orbitals calculated for the *N*-unsubstituted derivative **3b** (Figure 3) show that the non-degenerate HOMO level is stabilized relative to non-fused HPHAC (−4.37 eV) and is energetically well-separated from the H-1 level (by 0.56 eV). This feature is consistent with the

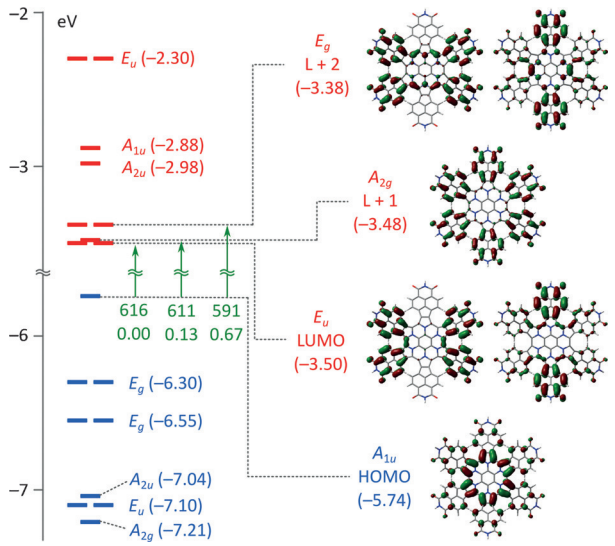

Figure 3. Kohn–Sham frontier molecular orbitals of **3b** at the B3LYP/6-31G(d,p) level of theory. Occupied and virtual levels are labeled in blue and red, respectively. Lowest energy electronic transitions, obtained from a time-dependent DFT calculation are shown in green along with predicted energies (in nanometers) and oscillator strengths.

observation of just two oxidations in **3a** and the increase of oxidation potentials relative to aryl-substituted HPHACs. Importantly, the fusion of NMI units to the HPHAC core considerably lowers the energy of frontier virtual levels, leading to a reduced band gap (2.24 eV vs. 3.06 eV in HPHAC) and enhanced electron affinity of the π system in **3a**. Remarkably, the four- and six-electron reduction pattern observed experimentally for **3a** can be correlated with the relative energies of virtual orbitals. The first six reductions can be tentatively associated with the nearly degenerate E_u (LUMO) and A_{2g} (L + 1) levels, whereas the L + 2 level (E_g), which is slightly higher in energy, can be linked to the subsequent four reductions.

Each of three lowest electronic transitions calculated for **3b** using time-dependent DFT is a pure excitation from HOMO to one of the lowest virtual levels. While the HOMO–LUMO transition ($A_{1u} \rightarrow E_u$) is dipole-forbidden, the $A_{1u} \rightarrow A_{2g}$ and $A_{1u} \rightarrow E_g$ transitions have nonzero oscillator strengths and are close in energy to the experimental absorption. The excitation from the HPHAC-centered HOMO orbital to one of the NMI-centered LUMOs results in a considerable charge-transfer (CT) character of the respective transitions. The charge is transferred in a radial fashion, likely producing a negligible net dipole moment in the excited state. Still, the π system undergoes considerable "radial" polarization, with the negative charge located on the periphery, a feature that is thought to contribute to the experimentally observed solvatochromism of **3a**.

In summary, we have described here the properties of a uniquely large, electron-deficient nanographene-like heterocycle based on the HPHAC motif. The concise synthesis of this species, which increases the number of fused rings from five to 37 in just two steps, illustrates the efficiency of assembling large aromatic targets by radial fusion. The warped, yet rigid surface of this new nanographenoid supports extensive solvation in the solid state and may serve as a scaffold for high-porosity materials. Without sacrificing the oxidation behavior inherited from its HPHAC parent, the new ring system reveals an exceptional ability to consecutively accept ten electrons at easily accessible potentials, yielding anions with small electronic band gaps and panchromatic UV/Vis-NIR absorption. Efficient aerial reoxidation of the reduced nanographenoid indicates its resistance to decomposition, making this new system of interest as a prospective functional dye.

Acknowledgements

Financial support from the National Science Center of Poland (grant numbers DEC-2012/07/E/ST5/00781, DEC-2014/13/B/ST5/04394 to M.S., and DEC-2015/19/N/ST5/00877 to M.Ż.K.) is gratefully acknowledged. Quantum chemical calculations were performed in the Centers for Networking and Supercomputing of Wrocław and Poznań.

Keywords: aromaticity · heterocycles · polyaromatic compounds · redox chemistry · synthesis

How to cite: *Angew. Chem. Int. Ed.* **2016**, *55*, 14658–14662
Angew. Chem. **2016**, *128*, 14878–14882

[1] A. Narita, X.-Y. Wang, X. Feng, K. Müllen, *Chem. Soc. Rev.* **2015**, *44*, 6616–6643.
[2] M. Stępień, E. Gońka, M. Żyła, N. Sprutta, *Chem. Rev.* **2016**, DOI: 10.1021/acs.chemrev.6b00076.
[3] M. Takase, V. Enkelmann, D. Sebastiani, M. Baumgarten, K. Müllen, *Angew. Chem. Int. Ed.* **2007**, *46*, 5524–5527; *Angew. Chem.* **2007**, *119*, 5620–5623.
[4] M. Takase, T. Narita, W. Fujita, M. S. Asano, T. Nishinaga, H. Benten, K. Yoza, K. Müllen, *J. Am. Chem. Soc.* **2013**, *135*, 8031–8040.
[5] E. Gońka, P. J. Chmielewski, T. Lis, M. Stępień, *J. Am. Chem. Soc.* **2014**, *136*, 16399–16410.
[6] M. Żyła, E. Gońka, P. J. Chmielewski, J. Cybińska, M. Stępień, *Chem. Sci.* **2016**, *7*, 286–294.
[7] H. Zhylitskaya, J. Cybińska, P. Chmielewski, T. Lis, M. Stępień, *J. Am. Chem. Soc.* **2016**, *138*, 11390–11398.
[8] H. E. Katz, A. J. Lovinger, J. Johnson, C. Kloc, T. Siegrist, W. Li, Y.-Y. Lin, A. Dodabalapur, *Nature* **2000**, *404*, 478–481.

[9] C. Wang, H. Dong, W. Hu, Y. Liu, D. Zhu, *Chem. Rev.* **2012**, *112*, 2208 – 2267.
[10] W. Jiang, Y. Li, Z. Wang, *Acc. Chem. Res.* **2014**, *47*, 3135 – 3147.
[11] J. Qi, W. Qiao, Z. Y. Wang, *Chem. Rec.* **2016**, *16*, 1531 – 1548.
[12] D. Bonifazi, M. Scholl, F. Song, L. Echegoyen, G. Accorsi, N. Armaroli, F. Diederich, *Angew. Chem. Int. Ed.* **2003**, *42*, 4966 – 4970; *Angew. Chem.* **2003**, *115*, 5116 – 5120.
[13] X. Wang, G. Sun, P. Routh, D.-H. Kim, W. Huang, P. Chen, *Chem. Soc. Rev.* **2014**, *43*, 7067 – 7098.
[14] H. A. M. Biemans, C. Zhang, P. Smith, H. Kooijman, W. J. J. Smeets, A. L. Spek, E. W. Meijer, *J. Org. Chem.* **1996**, *61*, 9012 – 9015.
[15] M. J. Turner, J. J. McKinnon, D. Jayatilaka, M. A. Spackman, *CrystEngComm* **2011**, *13*, 1804 – 1813.
[16] L. J. Barbour, *Chem. Commun.* **2006**, 1163.
[17] T. M. Long, T. M. Swager, *Adv. Mater.* **2001**, *13*, 601 – 604.
[18] N. T. Tsui, A. J. Paraskos, L. Torun, T. M. Swager, E. L. Thomas, *Macromolecules* **2006**, *39*, 3350 – 3358.
[19] F. Würthner, C. R. Saha-Möller, B. Fimmel, S. Ogi, P. Leowanawat, D. Schmidt, *Chem. Rev.* **2016**, *116*, 962 – 1052.

Received: August 28, 2016
Published online: October 14, 2016

